Journal of Applied Geophysics 95 (2013) 77–89

Contents lists available at SciVerse ScienceDirect

Journal of Applied Geophysics

journal homepage: www.elsevier.com/locate/jappgeo

Some considerations on electrical resistivity imaging for characterization of waterbed sediments

Luciana Orlando *

Department Ingegneria Civile Edile e Ambientale, Sapienza University of Rome, Via Eudossiana 18, 00184 Rome, Italy

ARTICLE INFO

Article history:
Received 21 February 2013
Accepted 8 May 2013
Available online 18 May 2013

Keywords:
Electrical resistivity imaging
Water-bottom survey
A priori constrains
1 and 2D modelling
Resolution
Waterbed sediments

ABSTRACT

The paper focuses on defining the performance and limits of ERI in the detection and sedimentary characterization of near-bottom thin layers. The analysis of the resolution of floating and submerged cables, and the effect of the accuracy of a priori information (resistivity and thickness) in the data inversion, is based on theory, models and actual data. Theoretical models show that the actual reconstruction of the near water-bottom sediments, in terms of geometry and resistivity, can be obtained only with the submerged cable, however, the data, unlike that acquired with the floating cable, require a priori information on water resistivity and thickness for the data inversion. Theoretical forward models based on wrong a priori water thickness and resistivity information influence the inverted model in different ways, depending on the under- and over-estimation of water resistivity and thickness, and the resistivity contrast of the water–solid layer; however a water–solid resistivity contrast of less than 2 and within 10% of error in water resistivity has no effect. Overestimating water resistivity depicts a ground similar to the actual ground in terms of resistivity, more so than the underestimation of water resistivity. Moreover, the data inversion is less influenced by water parameter error in the case of low resistivity contrast in the water–solid layer, than it is for high resistivity contrast. Wenner and Schlumberger arrays give comparable results, while a dipole–dipole array seems to be more sensitive to the accuracy of apparent resistivity measurements and a priori information on water.

The theoretical considerations were validated by actual data acquired with a submerged cable on the Tiber River. The study has shown that if highly accurate measurements are made of water thickness and resistivity, then electrical resistivity imaging from the submerged cable can be used in addition to, or even to substitute, seismic data for the reconstruction of the features and sedimentary characterization of near-bed sediments where seismic data fail to give a suitable resolution.

1. Introduction

In recent years geophysical methods have been commonly used to study alluvial plains, deltas and basins crossed by rivers, the depositional and erosive mechanisms of river sediments and erosion associated with bridge piers, pollutant infiltration, etc. Usually, single and multi-beam and side-scan sonars are respectively used for bathy-morphology studies and sedimentary characterization of river bed sediments, and single and multi-channel seismic methods are employed to investigate sedimentary deposits on the river bottom. Excellent results in terms of investigation depth (some hundred metres) and resolution have been obtained in big rivers like the Mississippi, the Hudson, and the Danube (Childs et al., 2003), where the sediments consist mainly of clay deposits.

Since 2002, I have been using seismic studies to investigate the hydrodynamics, sedimentology, stratigraphy, pollution, archaeology and navigability of the Tiber River (Bernabini et al., 2006; Bosman, 2004; Orlando, 2007; Orlando et al., 2003), but, unfortunately my studies, unlike those mentioned above, have not resulted in such excellent seismic data results for the lower course of this river (central Italy): Indeed, the near-water bed sediments are, for the most part, characterised by opaque seismic facies and high river-bed reflectivity, making it virtually impossible to define the sediment type (dense clay, cemented sand and/or gravel) (Bernabini et al., 2006).

The multi-fold data (Fig. 1a) show a low signal-noise ratio with low resolution and, in most cases, an investigation depth of a few metres; only in a few zones was the investigation depth 50–75 m (Orlando et al., 2003). Indeed, the single-fold data (Bernabini et al., 2006) provided higher resolution of the near surface sediments than did the multi-fold data (Fig. 1b and c).

To characterise the lithology and thickness of near water-bed sediments, I also used electrical resistivity imaging (ERI). This method has the potential to detect the near-bed layer with a resolution comparable to that of a seismic survey, and also gives information on sediment type.

* Tel.: +39 06 44585078; fax: +39 06 44585080.
E-mail address: luciana.orlando@uniroma1.it.

0926-9851
http://dx.doi.org/10.1016/j.jappgeo.2013.05.005

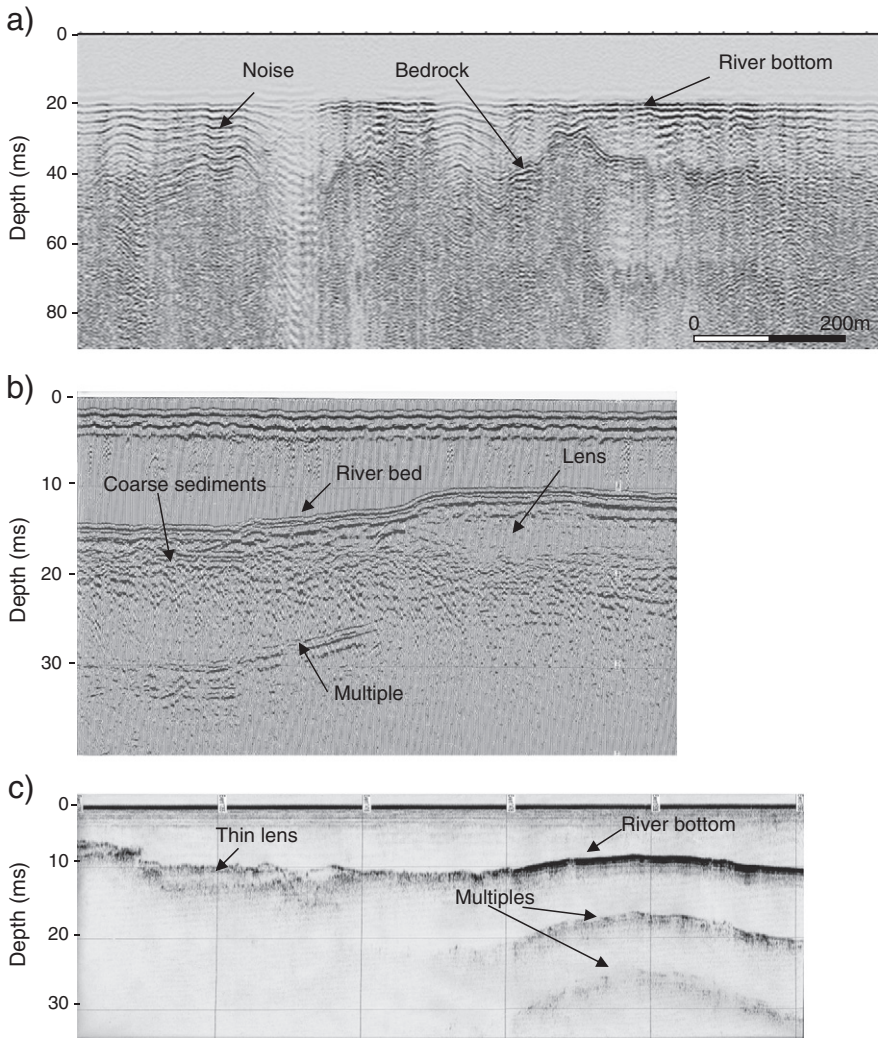

Fig. 1. a) Multi-fold seismic reflection section showing ringing and multiples; b) single-fold seismic section acquired with Sparker source showing lateral variation of type sediments; and c) single-fold seismic profile acquired with Pinger source showing clay lens.

Electric resistivity imaging with a floating cable was used by: Kwon et al. (2005) to study a fault zone underlying a river; by Snyder and Wightman (2002) to identify potential recharge areas; by Manheim et al. (2004) to detect fresh water lens; by Allen and Merrick (2006) to assess the connectivity between surface water and underground waters beneath rivers and channels; by Day-Lewis et al. (2006) for environmental purposes; and by Apostolopoulos et al. (2006) to study the geological setting of submerged marine sediments. Prior to the above studies Roy and Apparao (1971) stressed the dependence of resolution and investigation depth on water thickness, while Alfano (1962) and Snyder and Wightman (2002) demonstrated that the use of a submerged current electrode can, in part, by-pass the equivalence problem and increase the resolution. To increase the investigation depth Baumgartner (1996), and Baumgartner and Christensen (1998), developed a particular 1D method: electrodes placed in the water were aligned perpendicularly to the water level. This particular geometry allows the detection of the near-surface layer with good resolution, and increases the investigation depth. Some time ago Bernabini (1973) discussed vertical electrical soundings applied to a lake bed, and Scott and Maxwell (1989) multi-channel resistivity for mineral exploration in freshwater lakes.

The present paper discusses the possibility of using electrical resistivity imaging to complement, or replace, seismic data in investigating and characterising shallow sedimentary sequences, in cases where seismic investigation provides poor results. To define the performance and the limits of ERI in detecting near-bottom thin layers, I considered theoretical models with floating and submerged cables, and actual data acquired with submerged cable on the Tiber River. Moreover, I analysed the effect of the resistivity and the water thickness in the data inversion. I based the analyses of the resolution for the floating and submerged cables on one-dimensional master curves as they are easier to analyse than two-dimensional data and the conclusions are valid for 2 and 3 dimensional data. The effects on the data inversion of the accuracy of water-bottom topography and water resistivity were analysed on two-dimensional theoretical models. The theoretical considerations were validated by actual data acquired with a submerged cable on the Tiber River.

2. Theory and modelling

2.1. Modelling and analysis

From bibliography and theory, the latter discussed in Appendix A, I found that electrical resistivity imaging (ERI) acquired with floating and submerged cables can resolve, in different ways, the resistivity and thickness of near-bed layers, and for the submerged cable the

equivalence and/or instability problem in the data inversion can occur for wrong water parameter a priori constraints.

For an in-depth study, let us look at the following cases:

1. Sensitivity of floating and submerged cables in the detection of a middle thin layer;
2. Apparent resistivity of water–solid layer model for different, solid-layer resistivity and submerged cable;
3. Effect of a wrong water resistivity value on data inversion;
4. Effect of a small-scale wrong water-bottom topography on the data inversion;
5. Effect of a large scale wrong water-bottom topography on data inversion.

Cases 1 and 2 were analysed by calculating one-dimensional theoretical curves for horizontal stratified-layer earth models, the top layer (under the air half-space) consisting of water. The theoretical apparent resistivity curves were calculated using the finite difference algorithm, and were mapped on a logarithmic scale with the theoretical apparent resistivity to water ratio (ρ_a/ρ_w) versus the semi-distance of current electrode to water thickness (a/h_w) ratio.

The effects of wrong a priori water parameters (Cases 3–5) on the data inversion were analysed on two-dimensional models following this procedure: i) build up of 2-dimensional model, formed by 2 layers (water–solid) with submerged cable for Schlumberger spread; ii) calculation of apparent resistivity; iii) data inversion imposing wrong a priori constraint on resistivity or thickness of the water; and iv) analysis of results. The theoretical apparent resistivity and the data inversion were calculated using the finite-difference method implemented in the RES2DMOD and RES2DINV codes, commercialised by the Geotomo Corporation. A random noise level of 5% was added to the theoretical apparent resistivity. The apparent resistivity values were calculated with a forward modelling sub-routine (de Groot-Hedlin and Constable, 1990; Loke and Barker, 1996). The routine is based on a smoothness-constrained least-square method (de Groot-Hedlin and Constable, 1990; Sasaki, 1992).

Case 1. To test the performance of floating and submerged cables in detecting the thin layer lying below the water I calculated the apparent resistivity curves for the three layers, dipole–dipole and Schlumberger arrays (Fig. 2). The constitutive parameters of the model were: water thickness (h_w) and resistivity (ρ_w) equal to unity, thickness of layer 1 equal to $0.2h_w$ and resistivity of 0.1, 0.5, 2 and $10\rho_w$. Layer 2 was modelled with the same water layer resistivity (ρ_w). The apparent resistivity (Fig. 3) calculated for the model of Fig. 2 confirms that a dipole–dipole array is more sensitive to a middle-thin layer than a Schlumberger

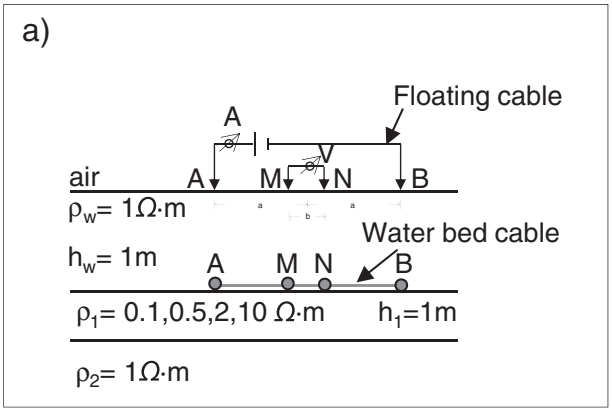

Fig. 2. Earth model and electrode setting for floating and submerged cable used for theoretical master curves of Fig. 4.

array for both floating and submerged cables. A middle-thin layer with $\rho_1 = 0.1\rho_w$ (Fig. 3a) is detectable with floating and submerged cables and both arrays. The apparent resistivity of the model with a thin-middle layer of $\rho_1 = 0.5\rho_w$ (Fig. 3b) is too small to be detected by a floating cable. A middle-thin layer with a resistivity of $2\rho_w$ (Fig. 3c) is detectable with a dipole–dipole array by both floating and submerged cables, while it is not detectable by Schlumberger array with a floating cable; for resistivity of a thin-middle layer equal to $10\rho_w$ (Fig. 3d), the floating cable seems to be more sensitive than the submerged cable for both arrays. The theoretical curves show that in the case of a small resistivity contrast of the water-middle layer, there is difficulty in detecting the middle layer for the floating cable with both Schlumberger and dipole–dipole arrays; the phenomenon is more evident when the middle layer is less resistive than the water (Fig. 3b). A middle layer of very high resistivity (compared to water resistivity) gives comparable curves (Fig. 3d) for floating and submerged cables. If the objective of the survey is to characterise near-surface sediments, a submerged cable, rather than a floating one, is recommended. This is because the latter has well-known data inversion equivalence problems for the middle thin layer: indeed, a correct estimation of the resistivity of a near-bottom layer can only be obtained from data acquired with a submerged cable.

Case 2. Fig. 4 shows the apparent resistivity of a two layer model and Wenner array using a submerged cable (Fig. 4a). The apparent resistivity was calculated for a water layer thickness $h_w = 1$ m and resistivity $\rho_w = 1\ \Omega \cdot$ m, and resistivity (ρ_1) of the half-solid layer equal to 0.2, 0.3, 0.5, 0.7, 1.0, 2.0, 3.0, 5.0, 7.0, and $10\rho_w$ (Fig. 4b). For $\rho_1/\rho_w < 1$ the ρ_a curves are well separated, while for $\rho_1/\rho_w > 1$ the curves are close to each other, this phenomenon is more evident for a small electrode offset ($a/h_w \to 0$), and indicates that small errors in apparent resistivity and water resistivity measurements can induce a more significant error in the ρ_1 estimation for a layer more resistive than water, rather than vice versa. In the case of correct water resistivity estimation, the resistivity of the solid layer for $\rho_1/\rho_w < 1$ can be defined without any ambiguity also for a small electrode offset as the curves are well separated.

Case 3. The effect of a wrong water resistivity value on the data inversion was analysed for the models of Figs. 5a and 6a: the parameters were water thickness equal to 1 m for both models, and a water–solid layer resistivity ratio of 2 and 0.5, respectively. The apparent resistivity was inverted with wrong water resistivities of 0.5 Ω · m (Figs. 5b and 6b) and 1.5 Ω · m (Figs. 5c and 6c). In both cases the data inversion shows a stratified ground instead of one homogeneous layer. An underestimation of the water resistivity in the data inversion (Fig. 5b) reveals a near-bottom layer with resistivity (1 Ω · m) and thickness (1 m) similar to that of water. Overestimation of the water resistivity in the data inversion (Fig. 5c) detects two layers with resistivity very similar to the actual one, with the thickness of the near bottom layer being around 2 m. In the latter case, data inversion provides a near-bottom model more similar to the actual one.

Also in the case of water less resistive than the solid layer (Fig. 6), the inverted model obtained with wrong-water resistivity show a stratified ground instead of one solid layer. Underestimating the water resistivity (Fig. 8b) in data inversion generates a near-bottom water layer around 1 m thick with a resistivity of 20 Ω · m, instead of the 2 Ω · m of the constitutive model. In the case of overestimation (Fig. 6c), the resistivity variation is smaller (1.2–2.3 Ω · m) than for water resistivity underestimation and the resistivity of the near-bottom layer is underestimated (1.2 Ω · m) with respect to the true one. In both cases, the near-bottom layer has a thickness around 1 m, equal to that of water. In the case of water less resistive than the solid layer, the water resistivity error induces a more significant error in the resistivity estimation of the near-bottom water layer than for water which is more resistive than the solid layer. These results confirm the Fig. 15 graph: data inversion is more sensitive to

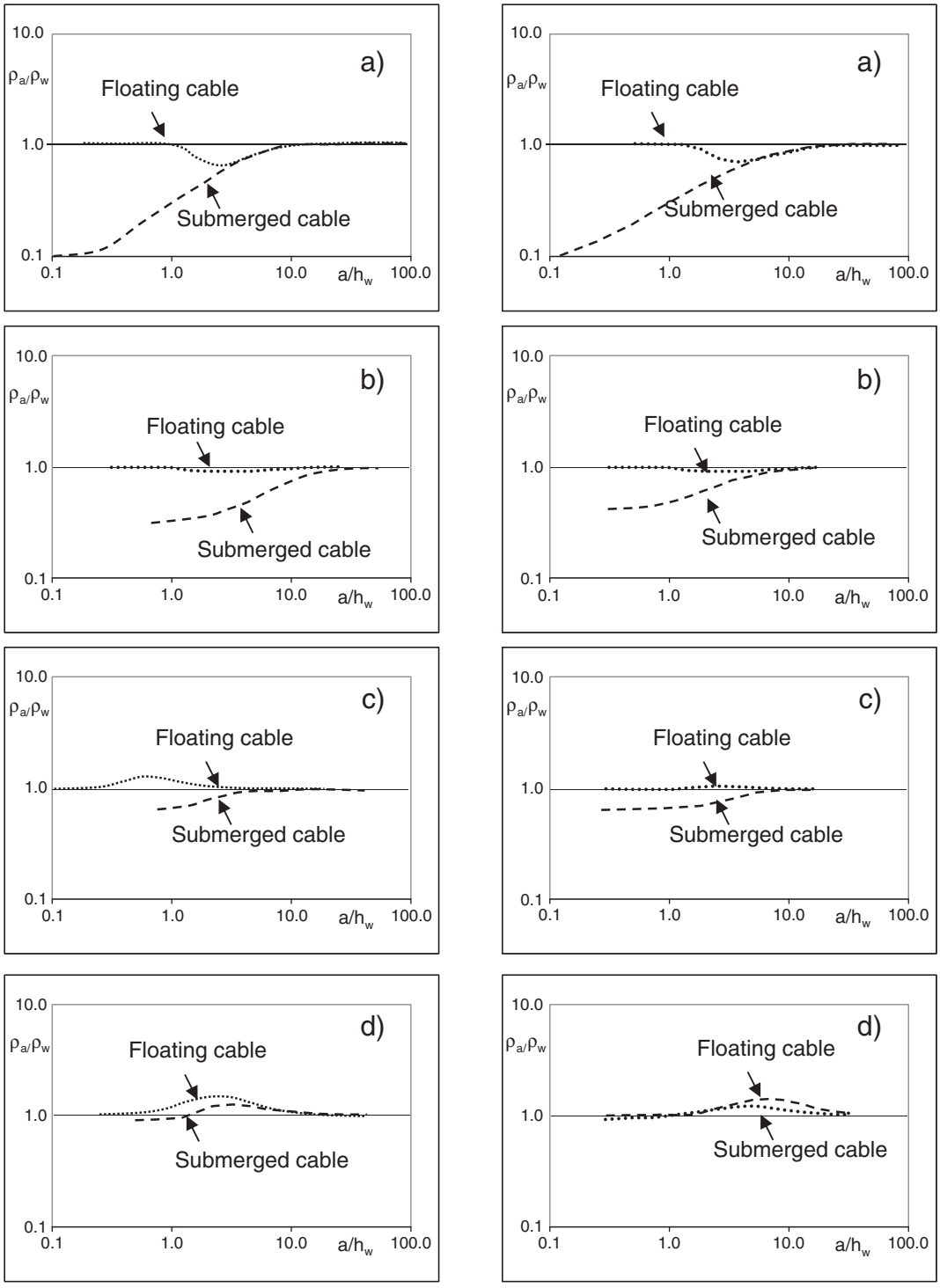

Fig. 3. Theoretical apparent resistivity curves for three layers: dipole–dipole (left) and Schlumberger (right) arrays with floating cable (dotted line) and with water bed cable (dashed line). Earth 1-dimensional model is described in Fig. 2. The first and third layers have equal resistivity, and the middle layer has resistivity of 0.5 (a), 0.1 (b), 2 (c) and 5 (d) times the water resistivity. The thickness of the second layer is 0.2 h_w.

error in estimating water resistivity for water which is less resistive than the solid layer, rather than vice versa.

Case 4. The topographic small-scale error of water thickness in the data inversion is analysed on models with water-bottom topography variations of 0.2, 0.4, 0.6, 0.8 m and water-layer resistivity contrasts of 2 and 0.5 (Figs. 7a and 8a). The apparent resistivity was calculated for electrode distances of 0.2, 1.0, 2.0 m, the electrodes being placed at the bottom of a 1 m thick water layer.

Data inversion was achieved by imposing the correct water resistivity and a 1 m thick flat water layer.

The inverted data (Figs. 7b,c,d and 8b,c,d) show that the non-modelled topography generates anomalies, with geometries similar to the non-modelled topography and a resistivity similar to that of water in both cases. Non-modelled small scale topography variations are detected differently, depending on the electrode offset: a 0.2 m electrode offset (Figs. 7b, 8b) is sensitive to all non-modelled topography variations; a 1.0 m electrode offset is sensitive to a topography variation

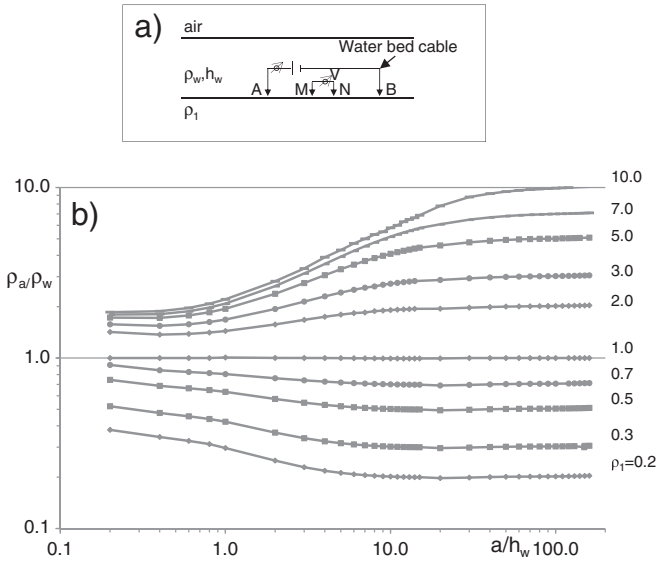

Fig. 4. a) Earth model and electrode setting used for theoretical apparent resistivity curves; b) theoretical apparent resistivity curves for water-bottom Wenner array. Water resistivity (ρ_w) of 1 Ω · m and thickness (h_w) of 1 m, and half layer resistivities of 0.2, 0.3, 0.5, 0.7, 1.0, 2.0, 3.0, 5.0, 7.0, and 10 ρ_w.

thicker than 0.4 m (Figs. 7c, 8c) and a 2 m electrode offset is barely sensitive to all the considered topography variations. Figs. 7 and 8 show that in the data inversion. From the previous results we can advance that a positive non-modelled topographic relief manifests itself in the inverted model as a less resistive anomaly than the solid layer in the case of a solid layer which is less resistive than water, and, as a more resistive anomaly, in the opposite case. In both cases the anomalies have shapes similar to the non-modelled topography.

Case 5. The topographic large scale error of water thickness in the data inversion is analysed on the models (Figs. 9a and 10a) for water–solid layer resistivity ratios of 2 and 0.5, respectively. Data inversion is achieved with water thicknesses 50% (Figs. 7b and 8b) and 150% (Figs. 9c and 10c) of the actual water thickness. Underestimation of water in the data inversion for a water–solid layer resistivity ratio of 2 (Fig. 9b) depicts a ground more similar to the actual one than the case of a 0.5 water–solid layer resistivity ratio (Fig. 10b); this is vice-versa when an overestimation of water thickness is imposed in the data inversion (Figs. 9c and 10c). Small-scale topographic errors induce anomalies in the same way as described earlier for both models.

The data of a model with a water–solid layer resistivity ratio of 2 (Fig. 9a), inverted with an underestimation of the water thickness (Fig. 9b), depicts a ground very similar to the constitutive model in terms of geometry and resistivity, showing only a slight resistivity variation. Resistivity variation is larger than in the previous case of water thickness overestimation (Fig. 9c). In the model with a 0.5 water–solid layer resistivity ratio (Fig. 10), the vice versa occurs.

These results show that the water thickness error in data inversion varies, depending on the water–solid layer resistivity ratio: for ratio >1, the underestimation of water thickness is less significant than in the case of overestimation; for ratio <1 the vice-versa occurs.

3. Discussion

The theoretical resistivity curves show that for a thin layer, with low resistivity contrast of the water–solid layer, a submerged cable allows a more accurate measure of the resistivity of the solid layer than a floating cable. The accuracy of the resistivity measurement of the solid layer also depends on the layer resistivity and electrode spread: a small resistivity contrast in the water–solid layer requires a more accurate measurement. For a submerged cable, the near-bottom solid layer can be univocally resolved, in terms of resistivity and thickness, only when both resistivity and water thickness are known, and equivalence problems are occurring only for the other solid layers.

Error in estimating water resistivity has a different effect in the data inversion: for water with less resistivity than the solid layer, water resistivity accuracy must be greater than for water with more resistivity than with solid layer resistivity. Such results confirm those of the theory

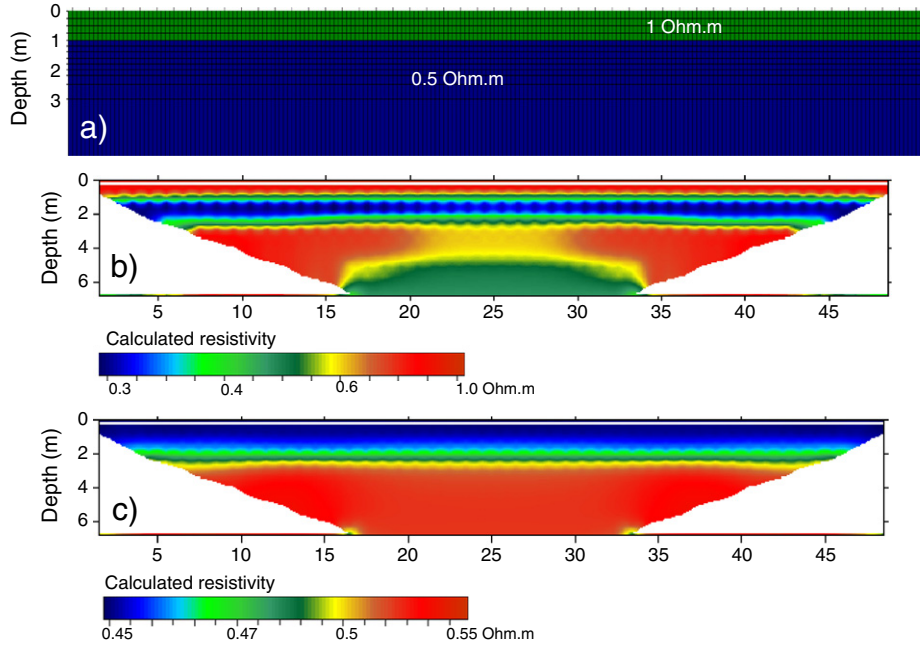

Fig. 5. a) Geometries and constitutive parameters of model. The resistivity contrast of water–solid layer is 0.2. Calculated resistivity for Schlumberger array with electrodes offset of 1.0. The data inversion was constrained with the wrong water resistivity: −0.5 m (b) and 1.5 m (c).

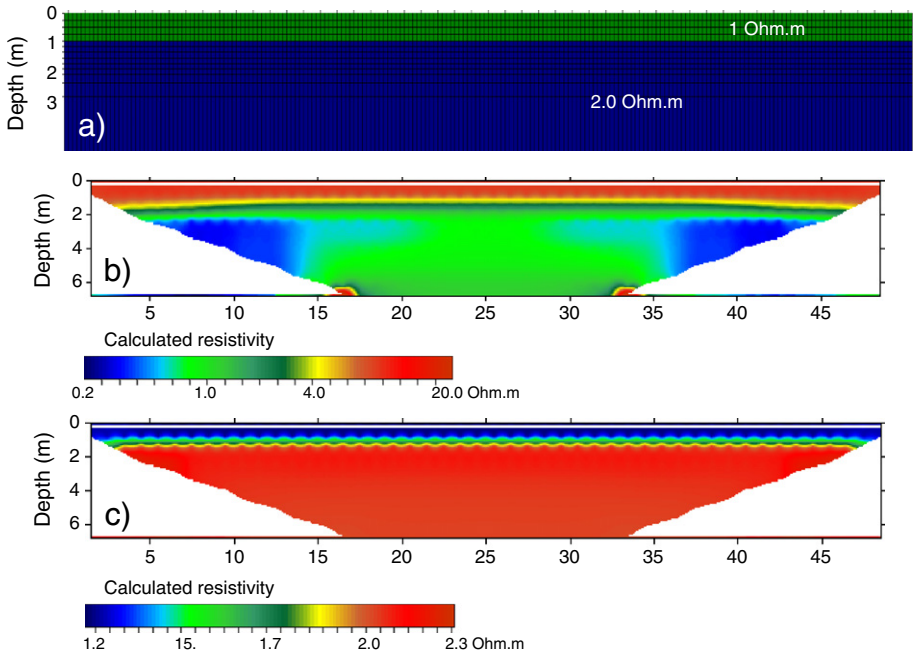

Fig. 6. a) Geometries and constitutive parameters of model. The resistivity contrast of water–solid layer is 2. Calculated resistivity for Schlumberger array with an electrode offset of 1.0. The data inversion was constrained with the wrong water resistivity of 0.5 m (b) and 1.5 m (c).

that data inversion is more sensitive to an underestimation of water resistivity than to an overestimation. The accuracy of small-scale water thickness depends on the electrode offset and the resistivity contrast of the water–solid layer. Large-scale error in water thickness in data inversion acts differently, depending on the water–solid layer resistivity ratio: for ratio >1, the underestimation of water thickness is less significant than in the case of overestimation; for ratio <1 the vice-versa occurs.

The theoretical study reveals that the choice between floating and sub-merged cables in the ERI method is not a simple task, and must the planned while taking into account several parameters as objectives of the survey, water depth and resistivity, thickness and resistivity of

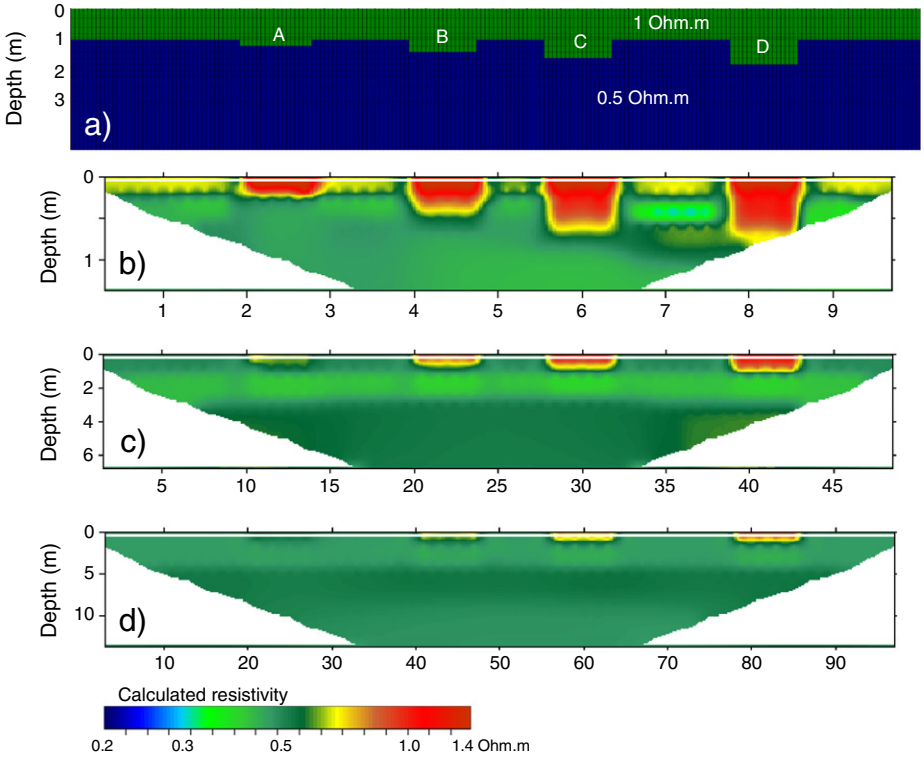

Fig. 7. a) Geometries and constitutive parameters of model. The resistivity contrast of water–solid layer is 0.2. The topography variations are 0.2, 0.4, 0.6 and 0.8 m (A, B, C, D, in figure a); calculated resistivity for Schlumberger array with an electrode offset of 0.2, 1.0 and 2.0 m, in b, c and d respectively.

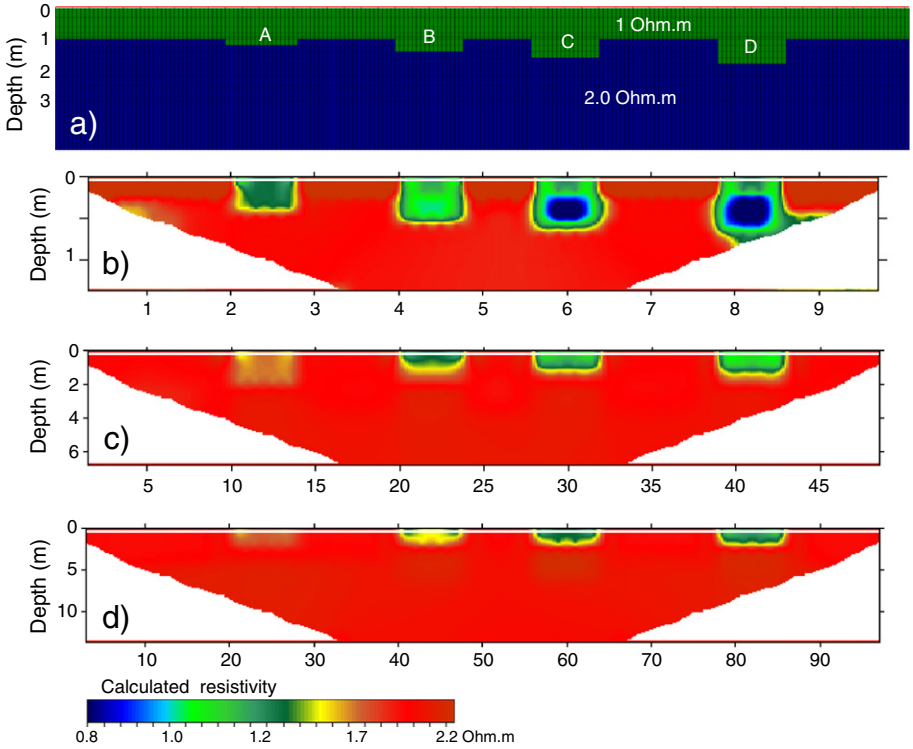

Fig. 8. a) Geometries and constitutive parameters of model. The resistivity contrast of water–solid layer is 2. The topography variations are 0.2, 0.4, 0.6 and 0.8 m (A, B, C, D, in figure a); calculated resistivity for Schlumberger array with an electrode offset of 0.2, 1.0 and 2.0 m, in b, c and d respectively.

the near-bottom layers, etc. To detect a thin layer close to the water bottom, a submerged cable is recommended, especially for a low resistivity ratio of the water–solid layer. The inversion of data acquired with a submerged cable needs to constrain the water resistivity and the positioning of the electrodes, both parameters must be accurate for a correct design of the geometry and resistivity of near-bottom stratigraphy. The discrepancy between the constitutive model and the model depicted by the data inversion depends on the resistivity accuracy and the water thickness, which in turn depend on the resistivity of the water–solid layer ratio.

4. Field data

4.1. Geological setting

The Tiber River has its source in the Fumaiolo Mountain and descends the Tuscan–Emilian Apennine chain to reach, after about 400 km, the city of Rome, from where it flows into the Tyrrhenian Sea. The first part of the Tiber flows parallel to the Apennine chain, which resulted from an extensional orogenic phase 5 million years ago. In the Rome area, where the geophysical surveys were performed, the river

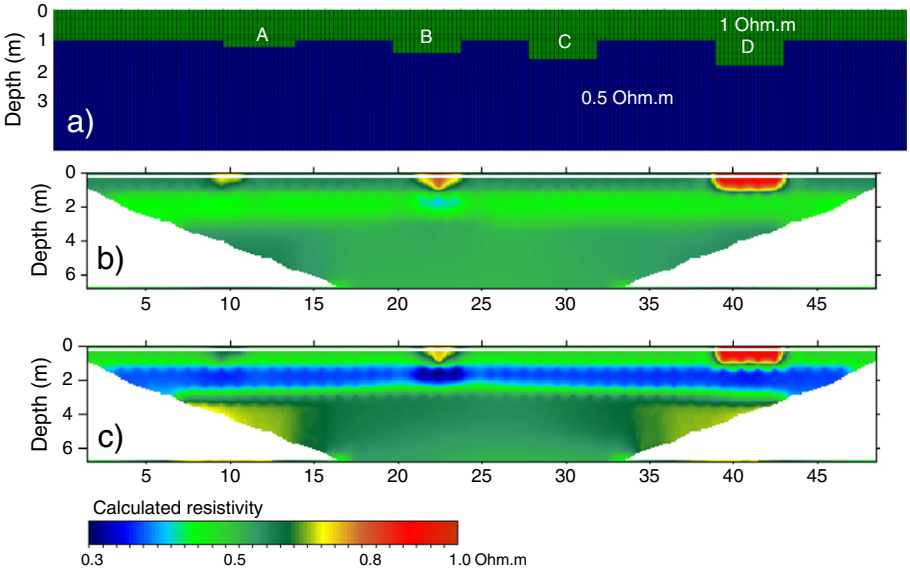

Fig. 9. a) Geometries and constitutive parameters of model. The resistivity contrast of water–solid layer is 0.2. The topography variations are 0.2, 0.4, 0.6 and 0.8 m (A, B, C, D, in figure a); calculated resistivity for Schlumberger array with an electrode offset of 1.0. The data inversion was constrained with the wrong water thickness: 0.5 m (b) and 1.5 m (c).

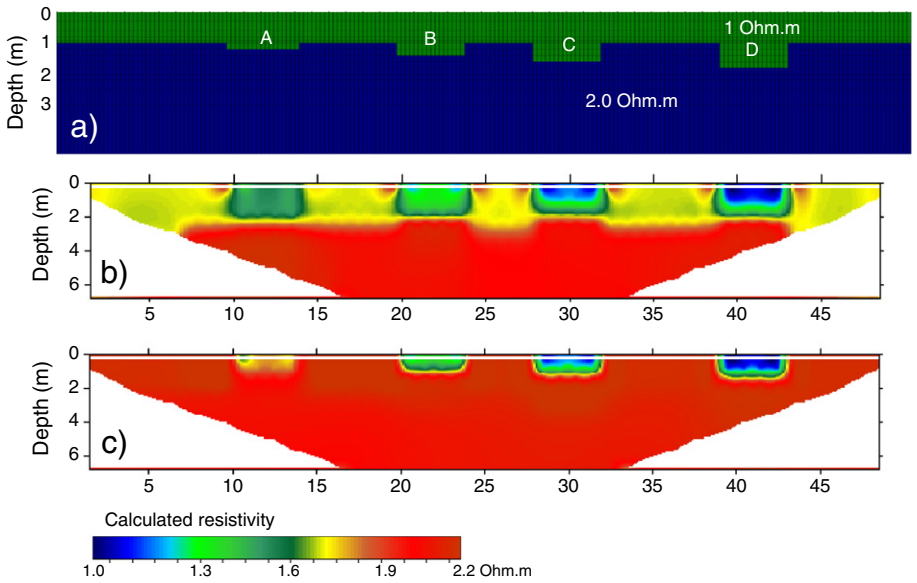

Fig. 10. a) Geometries and constitutive parameters of model. The resistivity contrast of the water–solid layer is 2. The topography variations are 0.2, 0.4, 0.6 and 0.8 m (A,B,C,D, in figure a); calculated resistivity for Schlumberger array with an electrode offset of 1.0. The data inversion was constrained with the wrong water thickness: 0.5 m (b) and 1.5 m (c).

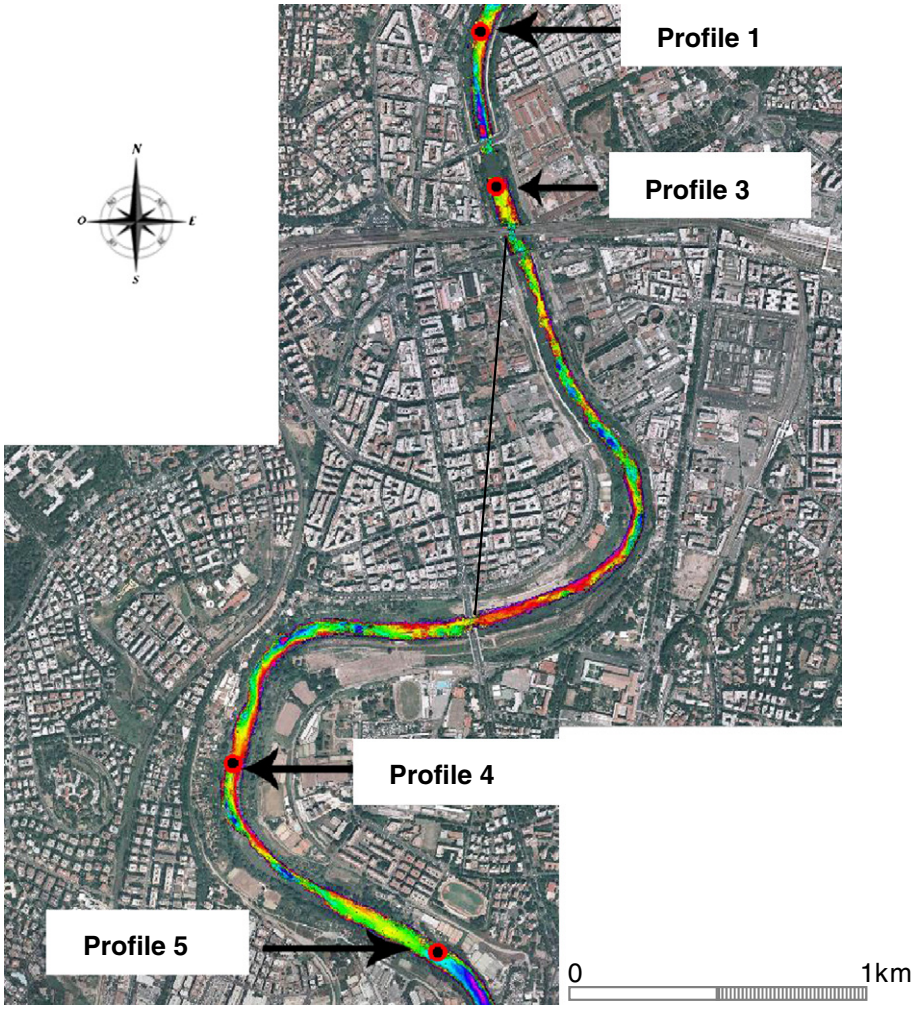

Fig. 11. Google Earth image of the study area with location of the electrical resistivity tomography and multi beam image. The ERI profiles are located in a lag of the Tiber River in Rome, downstream from Tiberina's Island which is 2 km to the north.

crosses an alluvial plain at an average elevation of 15–20 m above sea level. The plain consists of Pliocene sediments, almost 800 m thick, formed mainly by sandy–clay formations. Over the last 800,000 years the Tiber River has been the cause of erosion and deposition in the area.

4.2. Data acquisition and processing

I surveyed the Tiber River bottom with 5 profiles acquired with Wenner, Schlumberger and dipole–dipole spreads, the surveyed site being an urban segment upstream from Tiberina's Island (Fig. 11). Profile 2 has no geo-reference in the figure as there were problems with the GPS positioning during data acquisition.

The data were collected with a Syscal Pro instrument (IRIS Corporation) equipped with 24 electrodes spaced 1 m apart. The cable was ballasted at four points to keep it steady and straight, and was held in place by buoys at both ends. The cable was positioned with a Real Time Kinematics (RTK) GPS receiver. During the data acquisition the water depth was measured with an echo-sounder, and water resistivity ($10\ \Omega \cdot m$) was assessed on samples. Data inversion was performed by imposing constant resistivity for the water layer, because several velocity profiles acquired during the multibeam survey, give a velocity variation of less than $+/-1$ m/s along the water column; water temperature (from the top of the water to the bottom) remained constant, and the ERI data were acquired in a few hours and far from the salt wedge.

The data inversion was obtained with the same code used for the theoretical modelling. As shown in the analysis of the theoretical modelling, ERI data inversion acquired with electrodes on the water-bottom requires a priori information on the resistivity and thickness of the water layer. In the present study the water layer was considered a constant thick layer, $10\ \Omega \cdot m$ resistive. The thickness was calculated from the mean echo-sounder measurements acquired during the electrode-cable positioning and the resistivity was measured on a water sample.

The error induced in the data inversion was evaluated, at most, 0.6 m, that is the maximum depth variation found in the topographic profiles of the electrical resistivity imaging extracted from the multibeam data (Fig. 12). The theoretical model reveals that such topographic variations could create anomalies located near the sediment top, the maximum thickness being 0.6 m and the resistivity similar to that of water.

4.3. Data analysis

The first step was to analyse the effect of wrong a priori information (water resistivity and thickness) on the inversion of actual data (Profile 1 in Figs. 11, 12) acquired with a Schlumberger spread. The evaluation of the effect of wrong water parameters is done by comparing data inverted with correct water thickness (4.5 m) and resistivity ($\rho_w = 10\ \Omega$) parameters (Fig. 13a) with data inverted using incorrect thickness and resistivity (Fig. 13b,c,d,e). The topography variation of the profile is around 0.4 m (Fig. 12). The theoretical modelling discussed earlier led us to advance the hypothesis that the anomalies A and B (Fig. 13a) were due to non-modelled topography, their resistivity

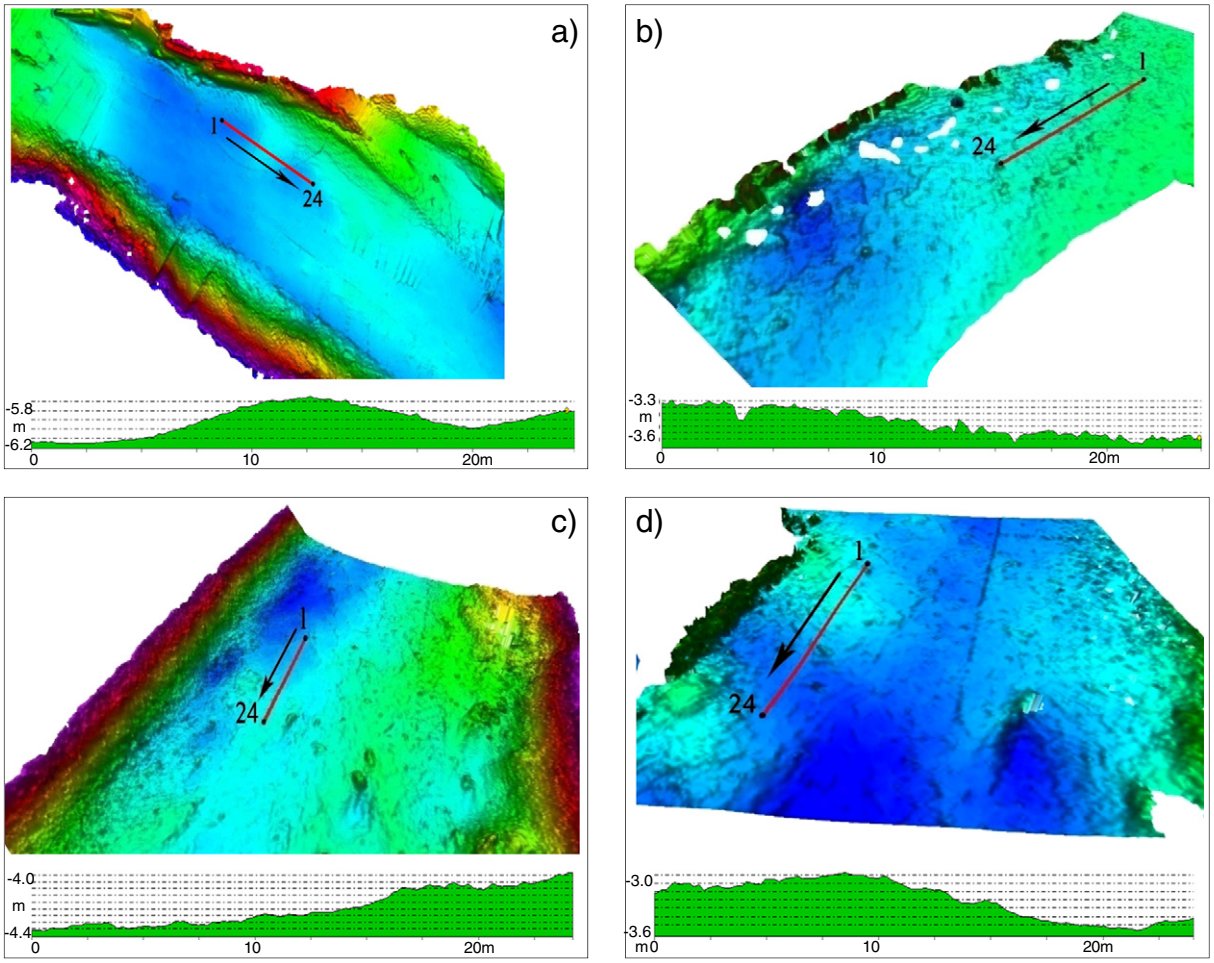

Fig. 12. Multi beam images of areas where we recorded electrical resistivity tomography Profiles 1 (a), 3 (b), 4 (c) and 5 (d). The lines indicate the tomography profile locations, the arrows indicate the direction. At the bottom of each the multi beam topographic profiles are shown.

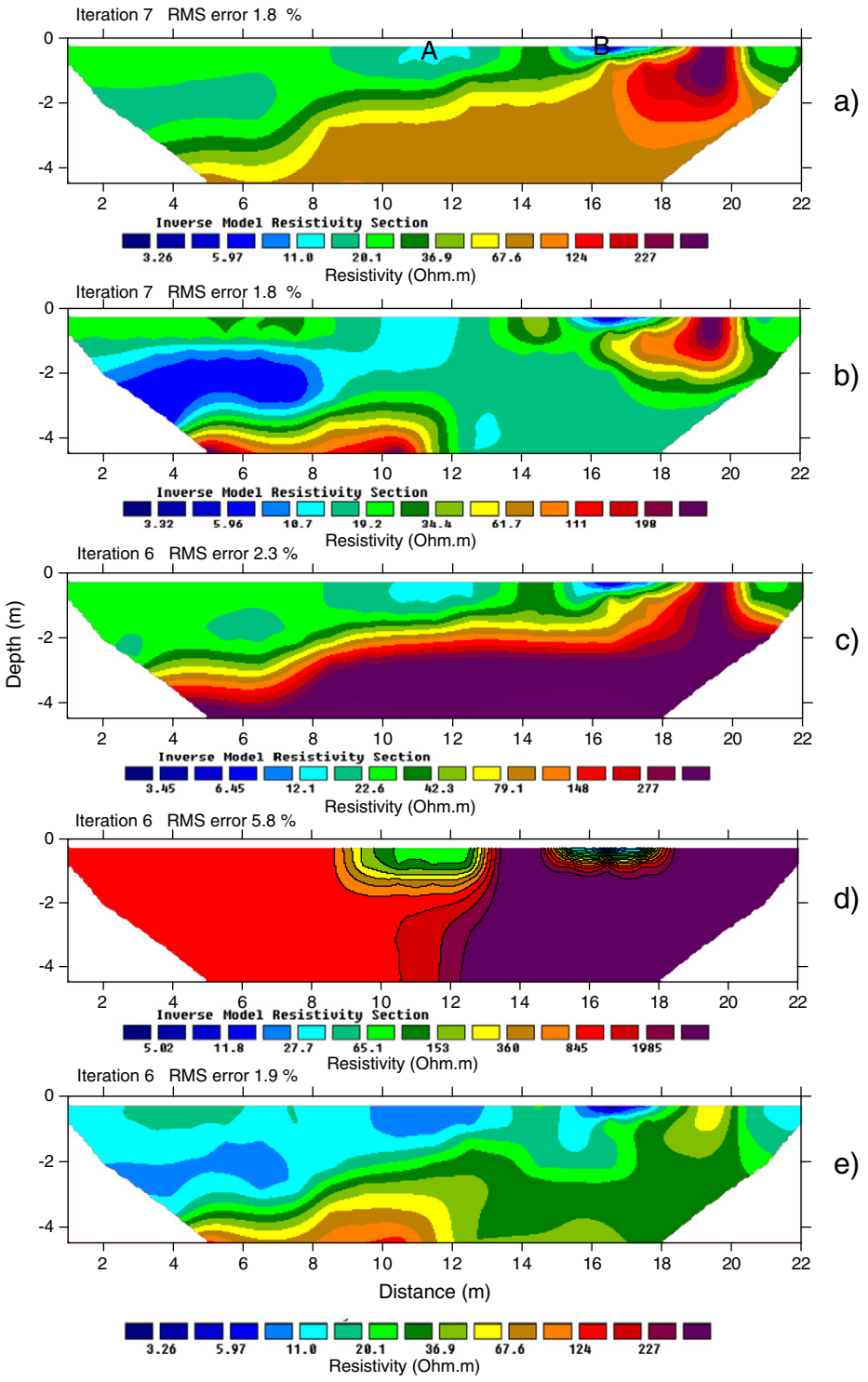

Fig. 13. Effects of incorrect a priori data (water resistivity and thickness) in the inversion of data of Profile 1. The data were acquired on the river bed with 24 electrodes, spaced 1 m apart, and a Schlumberger spread. a) Actual data inversion performed with the right thickness (4.5 m) and resistivity of water layer (10 Ω · m), right resistivity and incorrect thickness of 2.5 and 6.5 m (b and c) of water layer and right thickness and incorrect resistivities of 7 and 14 Ω · m of water layer (d and e). Note the change in the resistivity scale in d).

being similar to that of water. Wrong water thickness was analysed: incorrect water thicknesses of 2.5 and 6.5 m (Fig. 13 b, c) were applied to the data inversion. Underestimating (2.5 m) water thickness (Fig. 13b) depicts a ground with resistivity lower than the actual one (Fig. 13a), while overestimation of the water thickness (6.5 m) gives a setting and resistivity of the near-bottom ground very similar to that depicted by data inverted with correct parameters; in the deeper part the resistivity is higher than the correct one (Fig. 13c). Therefore overestimation of water thickness results in a better depiction of the setting and resistivity of the near bottom layer than its underestimation, a result that agrees with the theoretical one.

The effect of wrong water resistivity was analysed by imposing incorrect water resistivity, respectively 7 and 14 Ω · m (Fig. 13 d,e) in the data inversion. Comparing these data with those inverted with the correct parameters (Fig. 13a) shows that the underestimation of water resistivity (Fig. 13d) strongly influences the data inversion:

very high resistivity can be detected and severe instability is induced in the data inversion. Overestimating water resistivity results in a ground similar to that obtained on imposing correct water resistivity, and in this case the resistivity of the near-bottom layers is similar to that of water. These results are in a good agreement with the theoretical ones, and show that the sedimentary setting is less influenced by errors in the overestimation of water resistivity and thickness than by their underestimation. Error in the resistivity estimation of near-bottom sediments is smaller in the case of inaccuracy in water thickness than in water resistivity.

An analysis was made of electric resistivity profiles acquired with dipole–dipole (a), Schlumberger (b) and Wenner (c) spreads and inverted with correct water parameters. The results were similar for all the profiles, so let us look only at Profiles 3 and 4 (Fig. 14). To facilitate comparison, each profile, for all the spreads, is displayed with the same colour. The RMS (root-mean-square) error of data inversion is higher in the dipole–dipole spread than in the others. The Schlumberger (Fig. 14b) and Wenner (Fig. 14c) profiles are very similar, while the dipole–dipole (Fig. 14a) depicts a more complex ground and a wider resistivity range than the others.

Electric resistivity data investigated about 4 m of sediment, and detected 2 or 3 main layers (Fig. 14).

Dipole–dipole (a) detects one layer more than the Schlumberger (b) and Wenner (c) arrays. Note that Layer 1, detected by Schlumberger (b) and Wenner (c) arrays, is about 2.5–3 m thick and 30–40 Ω · m resistive, and Layer 2 has a resistivity >100 Ω · m. Instead the dipole–dipole arrays of Layer 1 show two sub-layers (1A and 1B), their resistivity being 40 Ω · m in the near bottom sub-layer and 10 Ω · m in the other, this latter being very similar to the resistivity of water. The dipole–dipole arrays detect two sub-layers near the water bottom, not the single layer detected by Schlumberger and Wenner, probably because of a higher sensitivity to error in a priori constraints on the resistivity and thickness of water.

No data was acquired for long electrode distances so there can be no definition of the true resistivity of the deeper Layer 2, as I already demonstrated theoretically.

This suggests the use of the resistivity values to calculate clay content only if the a priori information on water resistivity and thickness has been correctly surveyed.

5. Conclusion

I tested the limit and performance of ERI with 1-dimensional theoretical models for floating and submerged cables, information that can be considered valid also for 2- and 3-dimensional data.

Through theoretical modelling I have shown that the submerged cable is recommended to eliminate ambiguity when determining resistivity in near-bottom water sediments, especially for low water resistivity and solid layer contrast. In fact, in this case the floating cable was not able to detect layers of small thickness. On the other hand, submerged cable can be used for the correct estimation of resistivity of near water-bed sediments only if the resistivity and thickness of the water are known a priori. Indeed, a lack of accurate measurements concerning water depth and resistivity can lead to large errors in the data inversion.

2-D models with submerged cable show that a priori information on water resistivity and positioning of the electrodes must be accurately measured for the correct design of the geometry and resistivity of near-bottom stratigraphy. Error in the resistivity and setting of near-surface layers depends on the resistivity of the water–solid layer ratio and water thickness. In data inversion, error in water thickness can have different effects, depending on the water–solid layer resistivity ratio: for ratios >1, the underestimation of water thickness is less significant than in the case of overestimation; for ratios <1 the vice-versa occurs.

Actual data, acquired with submerged cable equipped with 24 electrodes spaced 1 m apart, show that the estimated resistivity of near-bed sediments is similar for Schlumberger and Wenner spreads. Dipole–dipole gives a greater-detail even if the resistivity is very close to that of water, and therefore appears far from the true resistivity. This study shows that ERI can characterise, in terms of resistivity and thickness, sediments near the water bottom, and resistivity can

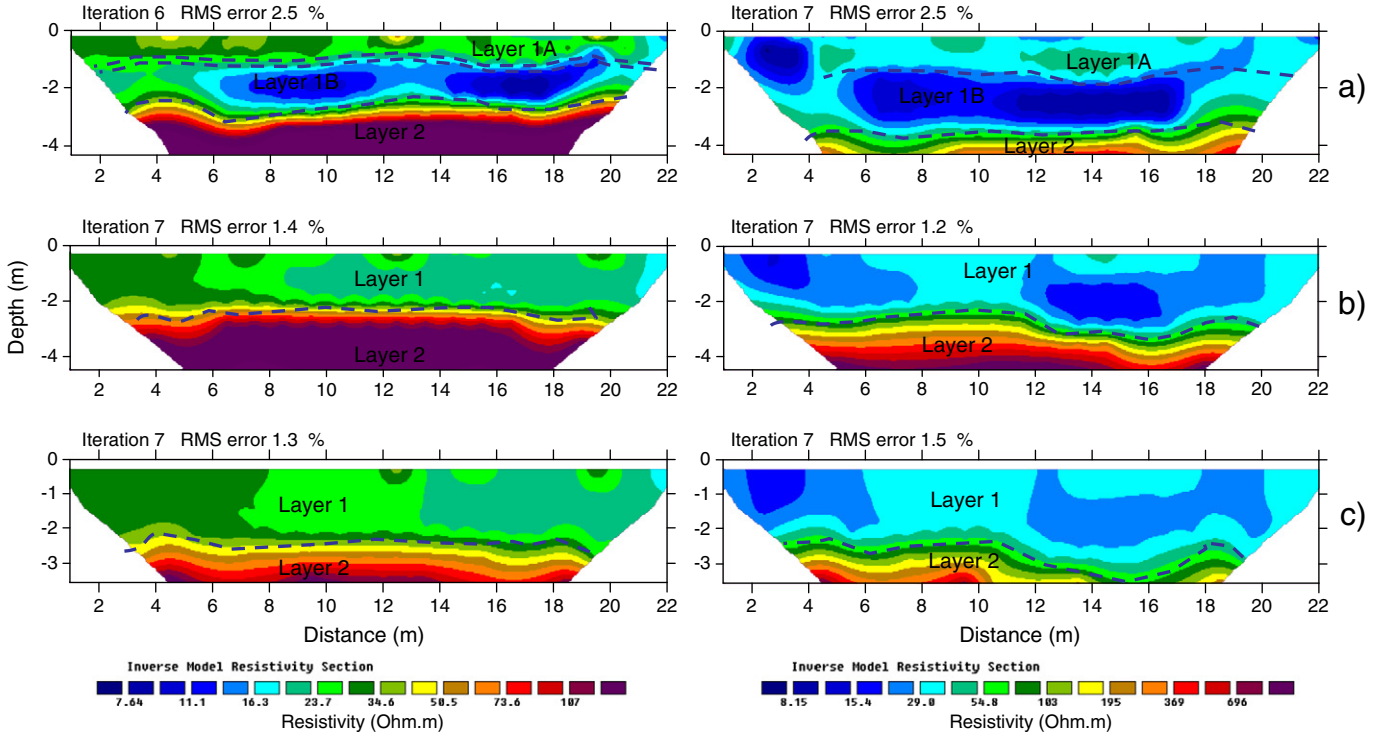

Fig. 14. Electrical resistivity imaging of Profile 3 (left); electrical tomography imaging of Profile 4 (right) acquired with dipole–dipole (a), Schlumberger (b) and Wenner spreads (c).

be used to estimate the transport of solid matter along the waterway, in an environmental impact assessment using a water-bottom cable. In a particular case like that of the Tiber, ERI data can give useful information, and this, integrated with seismic data, can help improve the knowledge of the sedimentary setting of the river.

A future project will be to validate the reliability of ERI in assessing the volume of clay in sediments sampled and analysed during electrical resistivity surveys, and to improve data quality, including the topography in the data inversion.

Acknowledgements

I wish to thank Professor M. Bernabini for his critical review, and Dr. Luigi Tramonti (Engineer) for his help with the data acquisition.

Appendix A

Theoretical analysis

Lagabrielle and Theilhaud (1981) and Lagabrielle (1983) comprehensively discussed the theory of electrical soundings of multi-layered earth with electrodes on the topographic surface and on the water bed floor. Their work followed that of Kunetz (1966) and, above all, Stefanescu and Schlumberger (1930).

Theories concerning electrical potential for one or two buried electrodes have appeared since the early 1960s (Alfano, 1962; Bhattacharya and Patria, 1968; Daniels, 1978, 1983; Merkel, 1971; Merkel and Alexander, 1971; Snyder and Merkel, 1973), but, to date, there has been no exhaustive discussion of electrical potential for four electrodes placed at the bottom of a water layer.

The potential difference ΔV between electrodes placed at the interface of two half-space layers with resistivities of ρ_w and ρ_1, and for an electrical current *I*, is given for the Wenner array with electrode distances *a* by

$$\Delta V = \frac{\rho_w \rho_1 I}{2\pi(\rho_w + \rho_1)}\left(\frac{1}{a}\right), \tag{1}$$

and for the Schlumberger spread with potential electrode separation *b* and current electrode separation *2 L* by

$$\Delta V = \frac{4\rho_w \rho_1 I}{\pi(\rho_w + \rho_1)}\left(\frac{b}{4L^2 - b^2}\right). \tag{2}$$

For both Wenner and Schlumberger spreads, the apparent resistivity (ρ_a) is given by

$$\rho_a = \frac{\Delta V}{I} C = \frac{\rho_w \rho_1}{(\rho_w + \rho_1)}, \tag{3}$$

where *C* is the array geometric constant that is equal to 2πL and $\pi L^2/b$ for Wenner and Schlumberger, respectively. Eq. (3) indicates that the apparent resistivity (ρ_a), for a two half-space layered model, is a function of ρ_w and ρ_1, and ρ_a is strongly influenced by the more conductive layer. The resistivity ρ_1 can be calculated knowing the apparent resistivity (ρ_a) and the resistivity of water (ρ_w) by

$$\rho_1 = \frac{\rho_w \rho_a}{(\rho_w - \rho_a)}. \tag{4}$$

Eq. (4) shows that the calculation of ρ_1 can be affected by instability in the case of ρ_a similar to ρ_w and the resistivity of water is not correctly evaluated.

I evaluated from relation (4), knowing the apparent resistivity (ρ_a), the effects in the estimation of the resistivity of the solid layer (ρ_1) for an incorrect water resistivity value (ρ_w) (Table 1). The normalised apparent resistivity (ρ_a/ρ_w) (column B in Table 1) was calculated for ρ_1/ρ_w equal to 10,5,2,1,0.5,0.2,0.1 (Column A in Table 1). The resistivity of the solid layer, ρ_1/ρ_{w_wrong}, was calculated for a water (ρ_{w_wrong}) resistivity error of −10, −5, 5 and 10% (columns C,D,E,F in Table 1). Fig. 15 shows ρ_1/ρ_{w_wrong} vs. ρ_1/ρ_w of Table 1. The graphs show that for $\rho_1/\rho_w < 2$, errors up to −/+10% of water resistivity estimation do not induce significant error in the ρ_1 calculation. The error is directly proportional to the resistivity contrast, and significant errors in the estimation of Layer 1 resistivity occur mainly because of the underestimation of water resistivity.

Table 1
Error in the resistivity estimation (ρ_1) of solid layer for two half-space models with electrodes on the interface induced by wrong water resistivity (ρ_w). All the values are normalised to ρ_w. A) Normalised solid-layer resistivity, B) apparent resistivities ($\rho_a = \rho_w \cdot \rho_1 / (\rho_1 + \rho_w)$). Resistivity of solid layer for error of −10% of ρ_w (C), −5% of ρ_w (D), 5% of ρ_w (E) and 10% of ρ_w (F) using the relation $\rho_1/\rho_w = \rho_a / (\rho_w - \rho_a)$.

A	B	C	D	E	F
ρ_1/ρ_w	ρ_a/ρ_w	ρ_1/ρ_{w_wrong}	ρ_1/ρ_{w_wrong}	ρ_1/ρ_{w_wrong}	ρ_1/ρ_{w_wrong}
10	0.909	−90.000	21.111	6.774	5.238
5	0.833	11.250	6.786	4.038	3.438
2	0.667	2.571	2.235	1.826	1.692
1	0.500	1.125	1.056	0.955	0.917
0.5	0.333	0.529	0.514	0.488	0.478
0.2	0.167	0.205	0.202	0.198	0.196
0.1	0.091	0.101	0.101	0.100	0.099

Following Stefanescu's method, the apparent resistivity of one-dimensional layers for a floating cable is given for Wenner and Schlumberger arrangements by the following relations respectively (Parasnis, 1997):

$$\rho_a(a) = 2a\rho_w \int_0^\infty K(\lambda)[J_0(\lambda a) - J_0(2\lambda a)]d\lambda, \tag{5}$$

and

$$\rho_a(L) = \rho_w L^2 \int_0^\infty K(\lambda) J_1(\lambda L)\lambda d\lambda, \tag{6}$$

where *a* is the electrode offset for the Wenner spread, *L* the half distance of current electrodes for the Schlumberger spread and $K(\lambda)$ the kernel function. Following the same procedure, for water bottom cables I obtained the same equation derived by Lagabrielle (1983) of apparent resistivity for Wenner and Schlumberger arrangements:

$$\rho_a(a) = \frac{2\rho_w \rho_1}{\rho_w + \rho_1} a \int_0^\infty K(\lambda)(J_0(\lambda a) - J_0(2\lambda a))d\lambda, \tag{7}$$

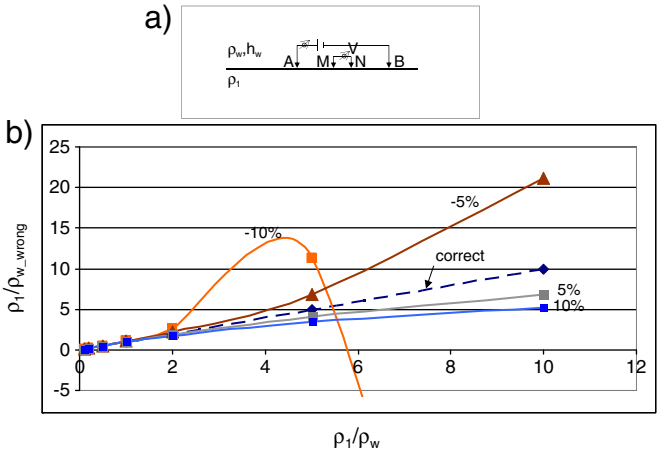

Fig. 15. a) Earth modelling used for theoretical apparent resistivity calculation; b) graph of $\rho_{1\_wrang} / \rho_{w\_wrong}$ vs. ρ_{1_wrong} / ρ_w for error of −10, −5.5 and 10% of water resistivity.

and

$$\rho_a(L) = \frac{\rho_w \rho_1}{\rho_w + \rho_1} L^2 \int_0^\infty K(\lambda) J_1(\lambda L) \lambda d\lambda, \tag{8}$$

respectively. For two and three layers, the Kernel functions ($K(\lambda)$) for a floating cable are given by:

$$K(\lambda) = \left(\frac{1 + K_1 e^{-2\lambda h_w}}{1 - K_1 e^{-2\lambda h_w}} \right), \tag{9}$$

and

$$K(\lambda) = \left(\frac{1 + K_1 e^{-2\lambda h_w} + K_1 K_2 e^{-2\lambda h_w} + K_2 e^{-2\lambda (h_1 + h_w)}}{1 - K_1 e^{-2\lambda h_w} + K_1 K_2 e^{-2\lambda h_w} - K_2 e^{-2\lambda (h_1 + h_w)}} \right). \tag{10}$$

For electrodes at the water bottom by:

$$K(\lambda) = \frac{1 + e^{-2\lambda h_w}}{1 - K_1 e^{-2\lambda h_w}}, \tag{11}$$

and

$$K(\lambda) = \left(\frac{1 + e^{-2\lambda h_w} + K_2 e^{-2\lambda h_w} + K_2 e^{-2\lambda (h_1 + h_w)}}{1 - K_1 e^{-2\lambda h_w} + K_1 K_2 e^{-2\lambda h_w} - K_2 e^{-2\lambda (h_1 + h_w)}} \right), \tag{12}$$

where, h_w is the water thickness, and ρ_w and ρ_1 are the resistivity of water and the solid half space-layer respectively. K_1 and K_2 are given by:

$$K_1 = \frac{\rho_1 - \rho_w}{\rho_w + \rho_1} \quad ; \quad K_2 = \frac{\rho_2 - \rho_1}{\rho_2 + \rho_1}.$$

The apparent resistivity (ρ_a) for floating and submerged cables differs because the ρ_w term of Eqs. (5), (6) is replaced by $\rho_1\rho_w / (\rho_w + \rho_1)$ in the relations (7) and (8), and in the Kernel function; the K_1 coefficient at the numerator of the second term is not present in the submerged cable Eqs. (11), (12). Because the inversion of data acquired with a submerged cable needs a priori information on the resistivity and thickness of water both these parameters may induce equivalence and/or instability problems in the reconstruction of the ground if they are not accurately measured.

Both the filter theory algorithm (Ghosh, 1971; Koefoed, 1979) and the iterative formula derived by Takahashi and Kawase (1990) can be used to calculate theoretical curves for horizontally stratified n-layer earth models for floating and submerged cables positioned at the water bottom. On comparing theoretical curves calculated with the Ghosh filter and with the finite difference algorithm (Loke and Barker, 1996) I obtained the same results. Therefore the present paper uses the finite difference algorithm for 1 and 2-dimensional theoretical calculations.

References

Alfano, L., 1962. Geoelectrical prospecting with underground electrodes. Geophysical Prospecting 10, 290–303.

Allen, D.A., Merrick, N.P., 2006. Robust 1D inversion of large towed geo-electric array datasets used for hydro-geological studies. Exploration Geophysics 38 (1), 50–59.

Apostolopoulos, G., Amolochitis, G., Stamataki, S., 2006. Marine resistivity tomography prior excavation works in port construction. EAGE 69th Conference, London 11–14 June 2007, p. E006.

Baumgartner, F., 1996. A new method for geoelectrical investigation underwater. Geophysical Prospecting 44, 71–98.

Baumgartner, F., Christensen, 1998. Analysis and application of a non-conventional underwater geoelectrical method in Lake Geneva, Switzerland. Geophysical prospecting 46, 527–541.

Bernabini, M., 1973. Electrical sounding on the bottom of a lake. Annali di Geofisica XXVI (2–3), 394–401.

Bernabini, M., Bosman, A., Chiocci, F.L., Macelloni, L., Orlando, L., 2006. Multi Beam and high resolution seismic reflection in the Tiber River. Proceeding of Near Surface Conference, Helsinki, 4–7 September, pp. 1–4.

Bhattacharya, P.K., Patria, H.P., 1968. Direct Current Geoelectric Sounding. Elsevier Science Publishing Co.

Bosman, A., 2004. Elaborazione ed integrazione di dati Side Scan Sonar e Multibeam ad alta risoluzione per lo studio di fenomeni d'instabilità gravitativa su edifici vulcanici insulari. Università di Roma Tor Vergata 1–150 (PhD Thesis).

Childs, J.R., Snyder, N.P., Hampton, M.A., 2003. Bathymetric and geophysical surveys of Englebright Lake, Yuba–Nevada Counties. California — US Geological Survey, Open-File Report 03-383.

Daniels, J.J., 1978. Interpretation of buried electrodes. Geophysics 42, 1006–1019.

Daniels, J.J., 1983. Hole-to-surface resistivity measurements. Geophysics 48, 87–97.

Day-Lewis, F.D., White, E.A., Johnson, C.D., Lane Jr., J.W., Belaval, M., 2006. Continuous resistivity profiling to delineate submarine groundwater discharge — examples and limitations. The Leading Edge 25 (6), 724–729.

de Groot-Hedlin, C., Constable, S., 1990. Occam's inversion to generate smooth, two dimensional models for magnetotelluric data. Geophysics 55, 1613–1624.

Ghosh, D.P., 1971. Inverse filter coefficients for the computation of apparent resistivity standard curves for horizontally stratified earth. Geophysical Prospecting 19, 769–775.

Koefoed, O., 1979. Geosounding Principles, 1. Elsevier Scientific Publishing Company, Amsterdam.

Kunetz, G., 1966. Principles of Direct Current Resistivity Prospecting. Gebrüder Bornträger.

Kwon, H.S., Kim, J.H., Ahn, H.Y., Yoon, J.S., Kim, K.S., Jung, C.K., Lee, S.B., Uchida, T., 2005. Delineation of fault zone beneath a riverbed by an electrical resistivity survey using a floating streamer cable. Exploration Geophysics 36, 50–58.

Lagabrielle, R., 1983. The effect of water on direct current resistivity measurement from sea, river or lake floor. Geoexploration 21, 165–170.

Lagabrielle, R., Theilhaud, S., 1981. Prospection de gisements alluvionnaires es site aquatique par profiles continues de resistivité au fond de l'eau. Bulletin de liason des Laboratoires des Ponts et Chaussées 114, 17–24.

Loke, M.H., Barker, R.D., 1996. Rapid least square inversion of apparent resistivity preseudosection of quasi-Newton method. Geophysical Prospecting 44, 131–152.

Manheim, F.T., Kranz, D.E., Brattan, J.F., 2004. Studying ground water under Delmarva coastal bays using electrical resistivity. Ground Water 42, 1052–1068.

Merkel, R.H., 1971. Resistivity analysis for plane-layer half-space models with buried current source. Geophysical Prospecting 19, 626–639.

Merkel, R.H., Alexander, S.S., 1971. Resistivity analysis for models of a sphere in half-space with buried current sources. Geophysical Prospecting 19, 640–651.

Orlando, L., Doglioni, C., Bernabini, M., Chiocci, F.L., Iannarilli, S., La Monica, G.B., Macelloni, L., Mariotti, G., 2003. Sismica a riflessione multicanale sul Fiume Tevere. Atti del 22° Convegno Nazionale del GNGTS, p. 420.

Orlando, L., 2007. Water bottom electrical tomography in the river Tiber. Proceedings of 69th of EAGE Conference & Exhibition. 10–13 June, 2007, London, pp. 1–4.

Parasnis, D.S., 1997. Principles of Applied Geophysics, Fifth edition. Chapman & Hall, London 121–155.

Roy, A., Apparao, A., 1971. Depth of investigation in direct current methods. Geophysics 36, 943–959.

Sasaki, Y., 1992. Resolution of resistivity tomography inferred from numerical simulation. Geophysical Prospecting 40, 453–464.

Scott, W.J., Maxwell, F.K., 1989. Marine resistivity survey for granular materials, Beaufort Sea. Canadian Journal of Exploration Geophysics 25, 104–114.

Snyder, D.D., Merkel, R.M., 1973. Analytic models for the interpretation of electrical surveys using buried electrodes. Geophysics 38, 513–529.

Snyder, D.D., Wightman, W.E., 2002. Application of continuous resistivity profiling to aquifer characterization. 15th SAGEEP Proceedings, Paper 13GSL10, 13.

Stefanescu, S.S., Schlumberger, C., 1930. Sur la distribution eléctrique potentielle autour d'une prise de ponctuelle dans un terrain à couches horizontal, homogènes et isotropes. Journal Physique et le Radium I 4, 132–140.

Takahashi, T., Kawase, T., 1990. Analysis resistivity in a multi-layer earth structure. IEEE Transaction on Power Delivery 5 (2), 604–612.